Future Trend in Seasonal Lengths and Extreme Temperature Distributions Over South Korea

Jangho Lee

School of Earth and Environmental Sciences, Seoul National University, Seoul, Korea

Abstract: CSEOF analysis is conducted on the daily mean, maximum, and minimum temperatures measured at 60 Korea Meteorological Administration stations in the period of 1979-2014. Each PC time series is detrended and fitted to an autoregressive (AR) model. The resulting AR models are used to generate 100 sets of synthetic PC time series for the period of 1979-2064, and the linear trends are added back to the resulting PC time series. Then, 100 sets of synthetic daily temperatures are produced by using the synthetic PC time series together with the The cyclostationary EOF (CSEOF) loading vectors. The statistics of the synthetic daily temperatures are similar to those of the original data during the observational period (1979-2064). Based on the synthetic datasets, future statistics including distribution of extreme temperatures and the length of four seasons have been analyzed. Average daily temperature in spring is expected to decrease by a small amount, whereas average temperatures in summer, fall and winter are expected to increase. Standard deviation of daily temperatures is expected to increase in all four seasons. The Generalized Extreme Value and Generalized Pareto distributions of extreme temperatures indicate that both warm and cold extremes are likely to increase in summer, while only warm extremes are predicted to increase significantly in winter. Thus, heat waves will increase and cold waves will decrease in number in future. Spring and fall will be shorter, whereas summer and winter will be longer. A statistical prediction carried out in the present study may serve as a baseline solution for numerical predictions using complex models.

Key words: Synthetic temperature, CSEOF, AR model, extreme value distribution, seasonal length

1. Introduction

It is well known that surface temperatures on global and regional scales have been increasing on a long-term scale due to global warming (Houghton et al., 2001). Due to global warming, observed annual mean temperature in Korea shows a warming trend over the past five decades (Jung et al., 2002; Kim and Roh, 2010). Not only the mean but also the variability of temperature has also increased (Luterbacher et al., 2004). Recent studies demonstrate that the occurrence of extreme temperatures including cold waves and heat waves has become more frequent (e.g., Schär et al., 2004). As reflected in many recent studies, extreme events in the last century are

of great concern both regionally and globally (Easterling et al., 2000; Bonsal et al., 2001; Walsh et al., 2001; Griffiths et al., 2005; Beinston et al., 2007). Griffiths et al. (2005) reported that change in mean temperatures could significantly affect the occurrence of extreme temperatures. In general, frequency of extremes exhibits a nonlinear relationship with changes in mean temperatures, and small changes in mean temperatures can result in significantly increased number of extreme events (Mearns et al., 1984). On the other hand, Katz and Brown (1992) demonstrated that change in the variance exerts stronger impacts on extreme events than the mean of temperatures.

In Korea, change in extreme temperatures has also been observed during the recent decades. Occurrence of extreme maximum temperatures, which are related to heat waves, tends to show an increasing trend. In contrast, occurrence of extreme minimum temperatures related to cold waves, shows a decreasing trend (Jung et al., 2002). Due to global warming and increased natural variability of temperature, it seems that the timing and length of the four seasons in Korea has also changed both in temperature and biology; earlier studies have already addressed that seasons are changing globally and regionally (Parkinson, 1994; Robenson, 2002; Meehl et al., 2007; Dwyer et al., 2012; Lynch et al., 2016).

The purpose of this study is to explore changes in daily temperatures, variance, and length of each season in South Korea, and to investigate the extreme temperature distributions in each season. Changes in the mean temperature, variance, onset date and length, as well as extreme value distribution for each season will be estimated for the next 50 years until 2064 based on the observed trends in the daily maximum, minimum, and mean temperatures. Earlier studies on the temperature change in Korea focused more on the annual mean temperature or the trend of temperature change. In the present study, however, more detailed patterns of temperature change are estimated by separating the four seasons. Furthermore, earlier studies on extreme temperature events in Korea focused more on the wintertime events. In this study, both summertime and wintertime extreme events are probed. Detailed statistical properties of extreme values are investigated by applying the extreme value theory such as the General Extreme Value (GEV) distribution and Generalized Pareto Distribution (GPD) (Gilleland and Katz, 2005). A statistical approach based on the KMA definitions of heat waves and cold waves are also used to investigate both

---

Corresponding Author: Jangho Lee, School of Earth and Environmental Sciences, Seoul National University, Seoul 08826, Korea.
E-mail: ilove9208@snu.ac.kr

summertime and wintertime extreme temperature events.

Section 2 shows the method of analysis used in this study. The cyclostationary EOF (CSEOF) technique is used as an important method of research, which allows a detailed representation of individual physical evolutions (Kim and Roh, 2010; Kim et al., 2013a, 2013b, 2014). The CSEOF method is useful for creating synthetic datasets, which are physically and statistically consistent with observational data (Kim and Wu, 1999). Hundred synthetic datasets will be constructed until 2064 based on the KMA observational data. Section 3a presents the results of CSEOF analysis with statistical comparisons between the synthetic datasets and the observational data. Synthetic datasets are validated through these statistical comparisons. In Section 3b, statistics including GEV and GPD distributions of the synthetic datasets for the present and the future periods will be presented and compared for the purpose of addressing future change in the statistics of daily temperatures. Summary and conclusions follow in section 4.

2. Data and Method of Analysis

a. Data

Data used in this study are the daily maximum, minimum and average temperature measurements at 60 Korea Meteorological Administration (KMA) stations during 1979-2014. The KMA stations are distributed fairly evenly over the southern part of the Korean Peninsula. A 365-day calendar is used by removing February 29 in the leap years.

b. CSEOF analysis

The primary analysis technique used in the present study is cyclostationary empirical orthogonal function (CSEOF) analysis (Kim et al., 1996; Kim and North, 1997; Kim et al., 2015). This technique writes space-time data in the form

$$T(r,t) = \Sigma_n B_n(r,t)T_n(t), \qquad t \in D \qquad (1)$$

where $B_n(r,t)$ are called cyclostationary loading vectors (CSLVs), $T_n(t)$ are called principal component (PC) time series, and r, t, n, D denote space, time, mode number and data interval, respectively. The crucial motivation for carrying out CSEOF analysis is to decompose data into a number of temporally evolving physical processes, $B_n(r,t)$, together with their amplitude time series, $T_n(t)$. Unlike conventional EOF analysis, each physical process is rendered as temporally evolving spatial patterns in CSEOF analysis. Further, CSLVs are periodic in time:

$$B_n(r,t) = B_n(r,t+d), \qquad (2)$$

where d is called the nested period. This is more appropriate representation of physical processes and facilitates the analysis addressed below.

c. Autoregressive (AR) modeling

Each PC time series is first detrended and is modeled as an AR process (Newton, 1988), that is,

$$\tilde{T}_n(t) = \Sigma_{j=1}^p \alpha_j \tilde{T}_n(t-j) + \varepsilon(t) \qquad t \in D \qquad (3)$$

where the trend, $tr_n(t)$, is removed from each PC time series, i.e.,

$$\tilde{T}_n(t) = T_n(t) - tr_n(t) \qquad (4)$$

Note that p is called an order, $\vec{\alpha} = \{ \alpha_j | j = 1, 2, \ldots, p \}$ are regression coefficients, and $\varepsilon(t)$ is a white noise process with a standard deviation σ. Then, $\tilde{T}_n(t)$ is referred to as an AR process and (2) is symbolically written as $\tilde{T}_n(t) \sim \text{AR}(p, \vec{\alpha}, \sigma)$. An AR modeling is to identify p, $\vec{\alpha}$, and σ such that the statistical properties of the model become identical with those of the original time series $\tilde{T}_n(t)$.

d. Prediction

Using the identified AR model, synthetic data can be generated as follows:

$$\hat{\tilde{T}}_n(t) = \Sigma_{j=1}^p \alpha_j \hat{\tilde{T}}_n(t-j) + \hat{\varepsilon}(t) \qquad t \in D+R \qquad (5)$$

where the hat sign signifies that the quantity is an estimation. In (5), $\{\hat{\tilde{T}}_n(t) | t = 1, 2, \ldots, p\}$ is assumed zero and $\tilde{T}_n(t = p+1)$ is estimated from a random value of a white-noise process $\hat{\varepsilon}(t)$ with variance σ^2. This procedure is continued until a sufficient number of time series is generated to cover the time period $D + R$, where R is the prediction interval abutting the data interval D. Typically the first D values of the estimated time series are discarded so that the effect of arbitrary initial conditions is eliminated. Then, the removed trend is added back to the estimated PC time series, that is,

$$\hat{T}_n(t) = \hat{\tilde{T}}_n(t) + tr_n(t), \qquad t \in D+R \qquad (6)$$

Finally, prediction data is constructed via:

$$\hat{T}(r,t) = \Sigma_n B_n(r,t) \hat{T}_n(t), \qquad t \in D+R \qquad (7)$$

Note that the estimated PC time series is used together with the loading vectors identified from CSEOF analysis of the KMA data. The resulting prediction data in (7) is consistent with the observational data both physically and statistically.
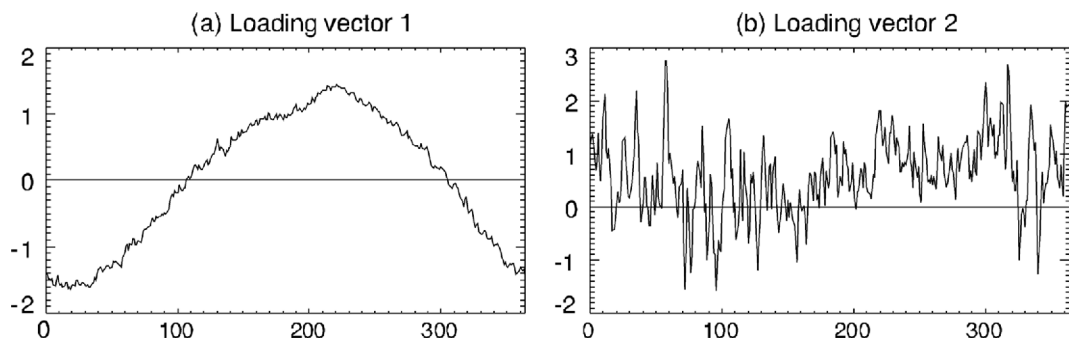
3. Results

a. Validation of synthetic datasets

CSEOF analysis was conducted on the KMA daily temperatures using the nested period of 365 days. By using the nested period of 365 days, we resolve any physical evolutions
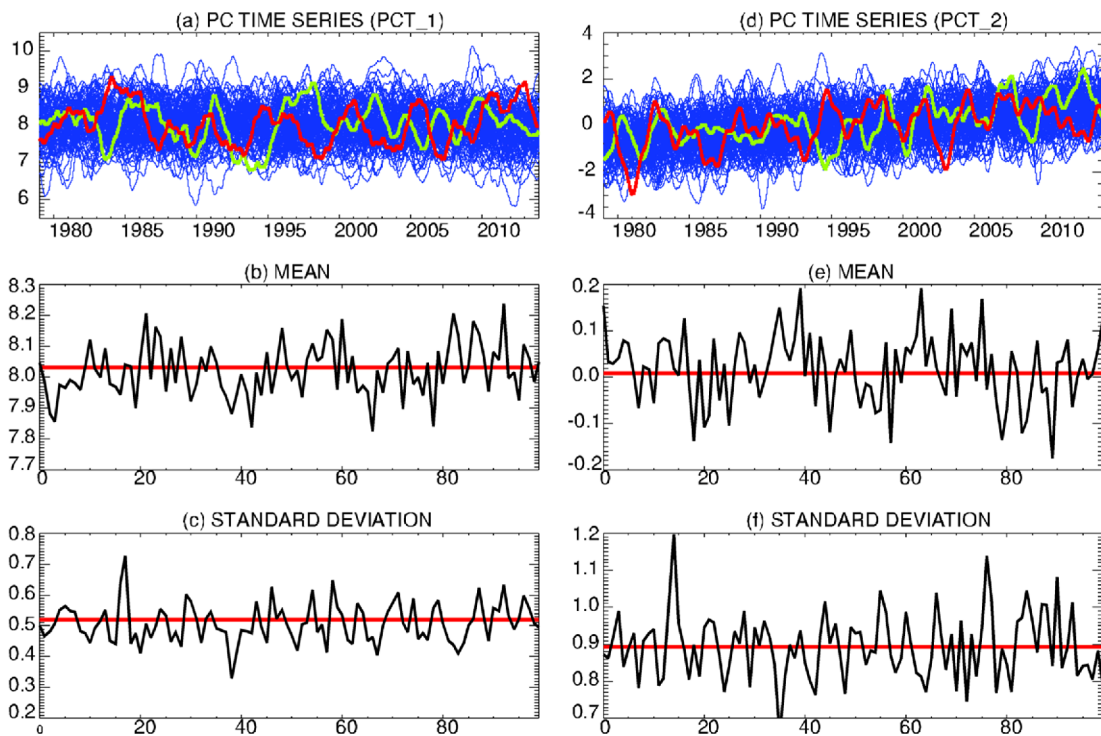
during the entire year. Figures 1 and 2 show the loading vectors and PC time series (red curves) of the first two CSEOF modes. The loading vector and the amplitude time series indicate that the first CSEOF mode is the annual cycle of daily maximum temperature in Korea and the second CSEOF mode is associated with regional warming. The amplitude of the annual cycle fluctuates by about ± 10% throughout the record period. It shows a typical seasonal variation of temperature throughout the year in Korea. The second CSEOF mode exhibits a conspicuous trend, which suggests that this mode is associated with warming of anthropogenic origin. As can be seen in the corresponding loading vector, the effect of warming is not uniform throughout the year. Rather, cooling is fre-

quently observed in March through June and briefly in November and December.

Synthetic time series were generated by using (5) and (6). Table 1 shows the AR order and noise variance for the first 10 PC time series. AR coefficients can be determined without any ambiguity from the PC time series once the AR order is given. Figure 2 shows the 100 synthetic time series of the first two PC time series over the period of 1979-2014. As can be seen in the figure, the magnitude of fluctuations is reasonably similar between the original and the synthetic time series. As should be expected, the trend of the original PC time series is nearly identical with those of the synthetic time series, which implies that the statistical properties of the original PC time series are
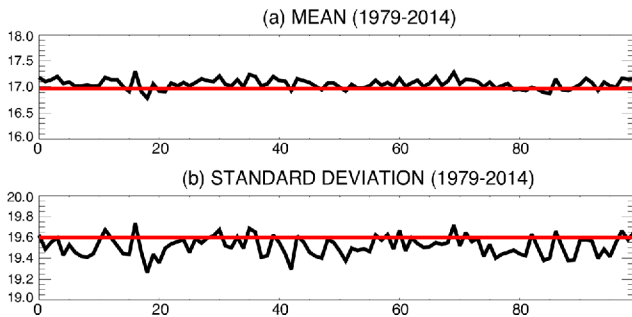

Fig. 1. The loading vector of the daily maximum temperatures averaged over the 60 KMA stations: (a) the first CSEOF mode, and (b) the second CSEOF mode.

Fig. 2. (a) The first PC time series of daily maximum temperature at the 60 KMA stations (red), 100 synthetic time series (blue), and one synthetic time series (green); (b, c) the mean and standard deviation of the first PC time series (red) and those of the 100 synthetic time series (black). (d, e, f) Same as (a, b, c) except for the second PC time series.

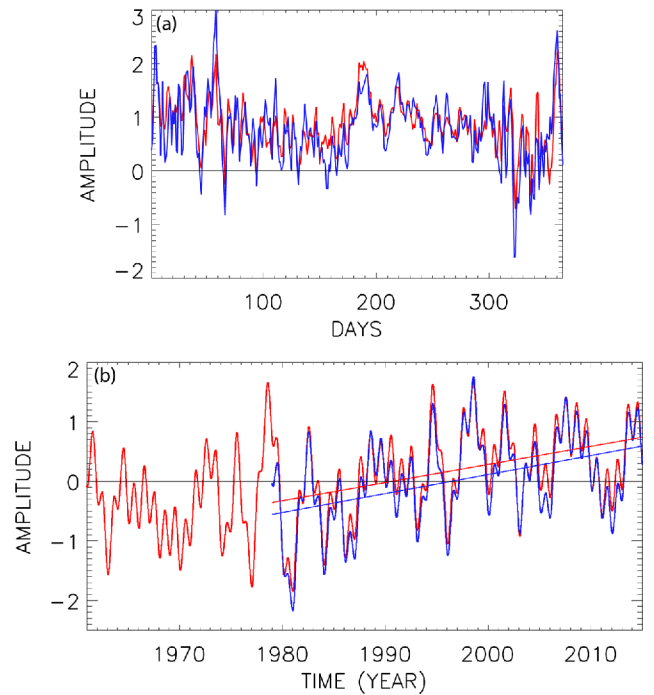**Table 1.** Values for order (p) and error variance (σ^2) for the first 10 PC time series.

	Max T		Mean T		Min T	
	p	σ^2	p	σ^2	p	σ^2
PC 1	28	0.0013	28	0.0016	28	0.0002
PC 2	25	0.0041	25	0.0036	25	0.0034
PC 3	5	0.0072	27	0.0009	28	0.0017
PC 4	28	0.0010	25	0.0017	27	0.0009
PC 5	33	0.0005	7	0.0062	8	0.0107
PC 6	5	0.0056	28	0.0011	27	0.0006
PC 7	27	0.0005	6	0.0031	11	0.0033
PC 8	4	0.0020	42	0.0001	28	0.0012
PC 9	25	0.0059	25	0.0035	28	0.0007
PC 10	27	0.0003	5	0.0029	27	0.0006

Fig. 3. (a) Mean and (b) standard deviation of daily maximum temperatures observed and averaged over 1979-2014 period at the 60 KMA stations (red), and those derived from the 100 synthetic datasets in the same period (black).

Fig. 4. (a) The loading vector and (b) PC time series of the KMA daily mean temperatures based on 1961-2014 record (red) and 1979-2014 record (blue). The black trend line is for the 1961-2014 record and the red and blue trend lines are for the two records for the period of 1979-2014.
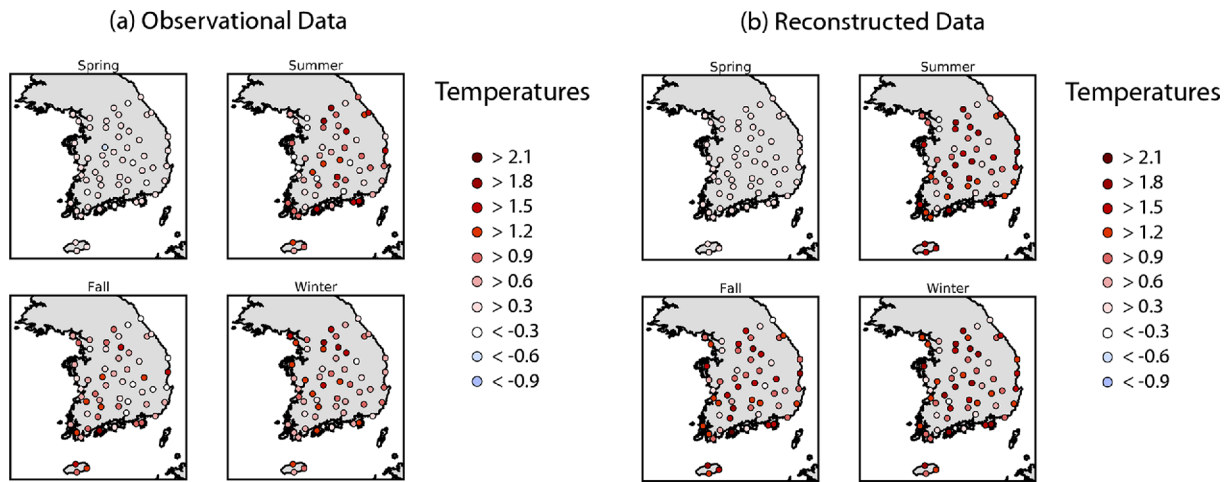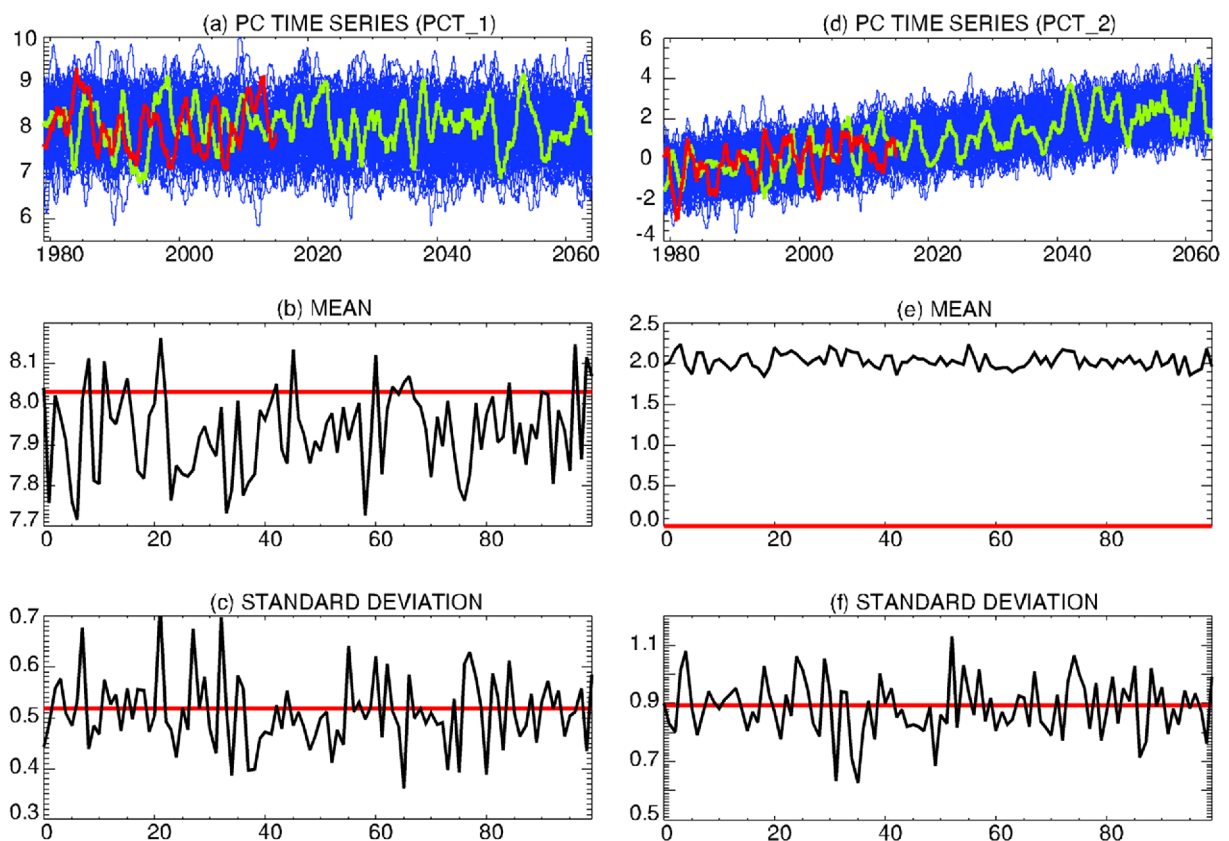
faithfully reproduced in the synthetic time series.

In the manner described above, synthetic PC time series are generated for the first 20 CSEOF modes; the first 20 CSEOF modes explain more than 90% of the total variability of KMA daily temperatures. A total of 100 sets of synthetic PC time series are produced in order to calculate the GPD and GEV distributions of extreme events with confidence. Then, synthetic daily maximum temperatures at the KMA stations are produced based on the 20 CSEOF modes by using (7). As can be seen in Fig. 3, the mean and standard deviation derived from the 100 synthetic daily maximum temperatures averaged over the KMA stations are nearly identical with those of the original data; each synthetic dataset seems to possess statistical properties similar to the original data.

While natural variability including Pacific Decadal Oscillation, Arctic Oscillation and El Niño Southern Oscillation can contribute to the local warming or cooling, its contribution to the warming mode should not be significant. In order to assess the contamination of the warming mode by natural variability, CSEOF analysis was conducted on longer (1961-2014) records at 15 KMA stations. As can be seen in Fig. 4, both the loading vector and the PC time series of the second CSEOF mode are similar to those based on a shorter (1979-2014) record; correlation for the loading vector is 0.82 and that for the PC time series is 0.98. The slope of the trend line based on the longer record is slightly less than that based on the shorter record; they are 2.25×10^{-2} and 3.05×10^{-2} per year, respectively. Thus, the difference in the amplitude can be 0.8 in a century. This implies that mean seasonal temperature can be off by 0.41, 0.26, 0.42, and 0.29 in winter, spring, fall, and winter, respectively. While this difference is not quite negligible, it is justifiable in the context of the statistical nature of the present study.

Figure 5 shows the temperature increase between the two periods, 2005-2014 and 1979-1988, from the KMA data and the reconstruction data based on the second CSEOF mode. As seen in the figure, the second CSEOF mode faithfully describes the trend in the actual data at all 60 KMA stations. The average temperature increases throughout all seasons. Temperature increase is low in spring, while it is relatively high in other seasons. The sign of change is nearly uniform throughout the Korean Peninsula, suggesting that the second mode characterizes a wide scale temperature change. In fact, the PC time series is highly correlated with that of the warming mode in Kim and Roh (2010); the warming mode in Kim and Roh was shown to represent a continental-scale warming (see Fig. 7 in Kim and Roh, 2010).

(a) Observational Data

(b) Reconstructed Data

Fig. 5. (a) Difference in observed average temperature between 1979-1988 period and 2005-2014 period; (b) same for the reconstructed data using the second CSEOF mode. Each season is divided according to months (Spring: March, April, May; Summer: June, July, August; Fall: September, October, November; Winter: December, January, February).
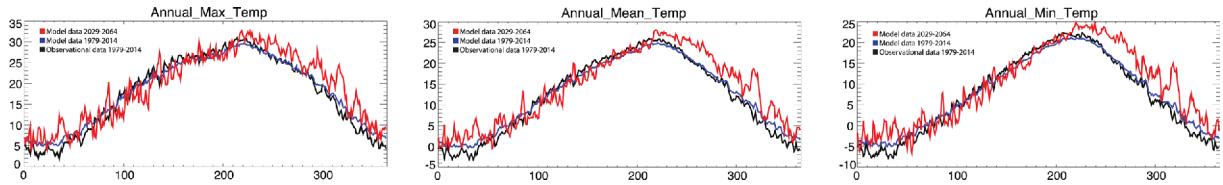

Fig. 6. (a) The first PC time series of the daily maximum temperatures at the 60 KMA stations (red), 100 synthetic time series (blue) and one synthetic time series (green) extended until 2064; (b, c) the mean and standard deviation of the first PC time series (red) and those of the 100 synthetic time series from 2029 to 2064 (black). (d, e, f) Same as (a, b, c) except for the second PC time series.
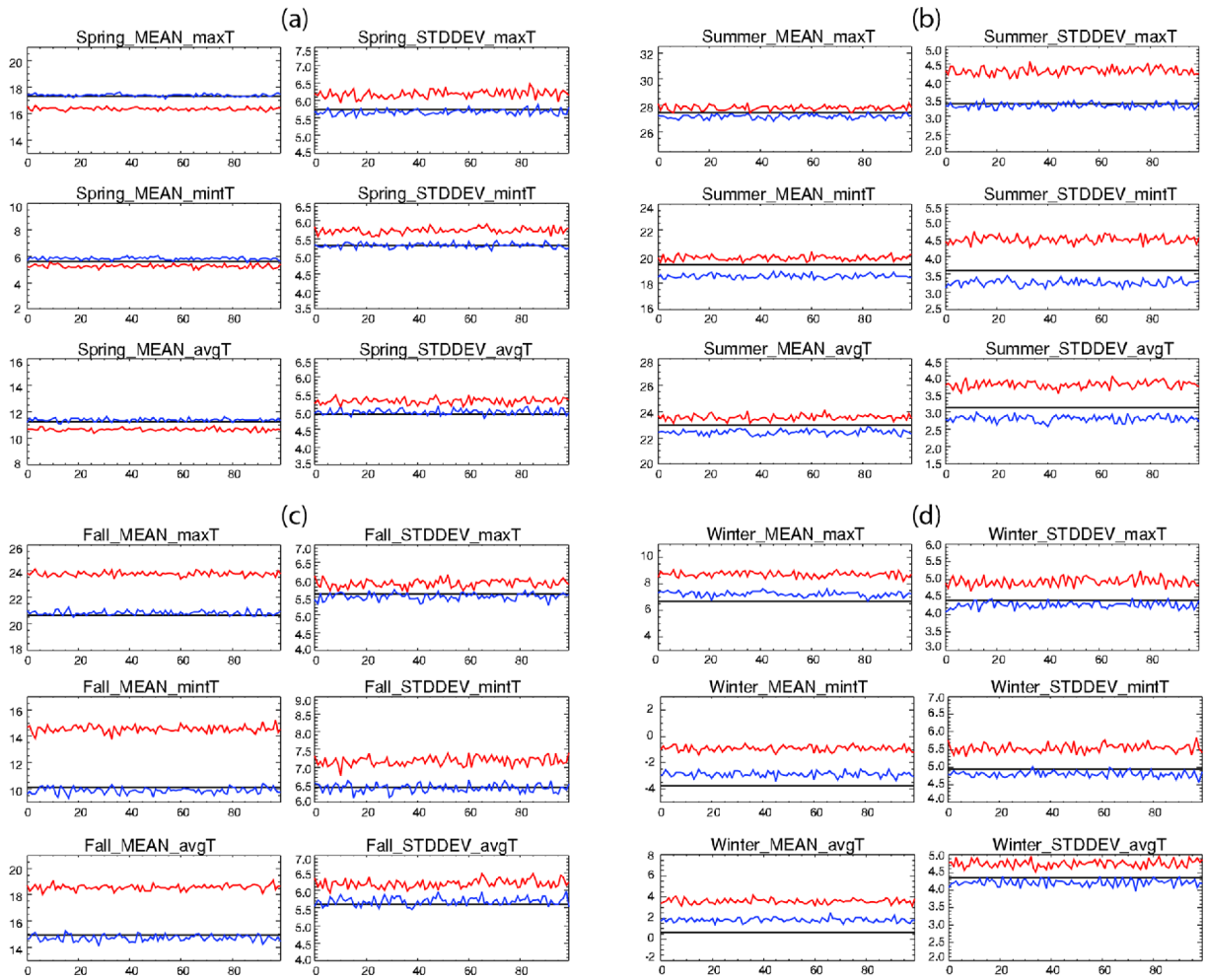
b. Future statistics

Figure 6 shows the extended synthetic PC time series over the period of 1979-2064. The envelope of the 100 synthetic time series shows a weak linear trend for the first CSEOF mode and a strong linear trend for the second CSEOF mode.

Fig. 7. The annual (or climatological) cycle for daily maximum, mean, and minimum temperatures averaged over all the 60 KMA stations: KMA observations (black), 100 synthetic datasets in 1979-2014 (blue) and 100 synthetic datasets in 2029-2064 (red).
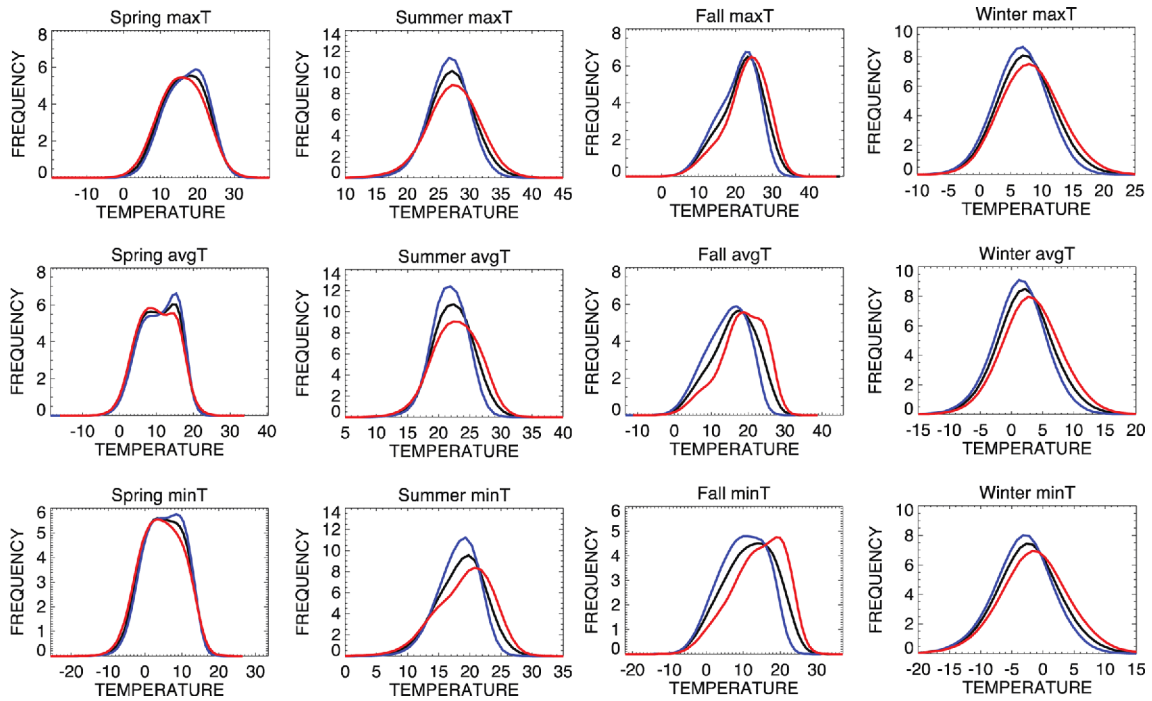

Fig. 8. The mean and standard deviation of maximum temperatures (upper), minimum temperatures (middle), and average temperatures (lower): observation in 1979-2014 (black), 100 synthetic datasets in 1979-2014 (blue) and in 2029-2064 (red). Panels (a)-(d) represent spring (3/1-5/30), summer (6/1-8/30), fall (9/1-11/30), and winter (12/1-2/28), respectively.

As seen in the figure, the amplitude of the annual cycle decreases slightly in time, while the amplitude of the warming increases significantly (Kim and Roh, 2010); the envelope of the 100 synthetic time series clearly shows the trend. These modes indicate that the amplitude of the annual cycle will become gradually weaker as warming proceeds further in future. The mean of synthetic time series also confirms these trends; the mean of the first CSEOF mode (annual cycle mode) in the future period (2029-2064) is less than that in the record

period (1979-2014), while that of the second mode (warming mode) is much stronger in the future period.

Figure 7 shows the climatological cycle of temperature for the synthetic data in comparison with that of the KMA data. As seen in the figure, the annual temperature evolution in the synthetic datasets is similar to that of the KMA data in the 1979-2014 period. On the other hand, the annual temperature evolution of the synthetic datasets in the 2029-2064 is remarkably different from that of the KMA data. In the future

Fig. 9. The histograms of daily temperatures derived from the 100 synthetic datasets during 1979-2014 (blue), 1979-2064 (black), and 2029-2064 (red). The four columns represent the spring (3/1-5/30), summer (6/1-8/30), fall (9/1-11/30), and winter (12/1-2/28), respectively. The ordinate represents the average frequency of occurrence for each season.

Table 2. Percentage of extreme events in the observational period and future period based on the KMA criteria and the $2\sigma(\mu \pm 2\sigma)$ criteria. The KMA criteria of heat wave is maximum temperature over 33°C and of cold wave is minimum temperature below −12°C.

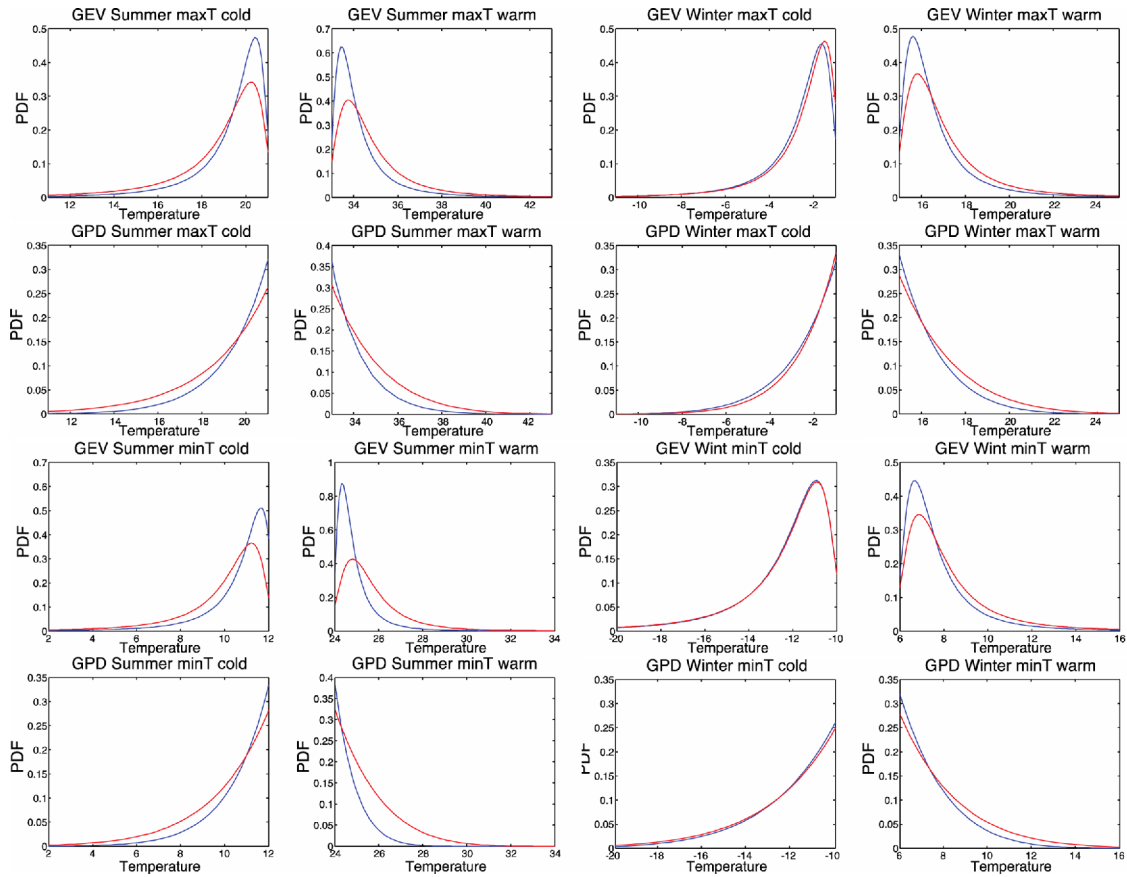|	Summer 1979-2014	Summer 2029-2064	Winter 1979-2014	Winter 2029-2064
Mean (μ)	27.15°C		−2.86°C	
Standard deviation (σ)	3.31		4.75	
KMA criteria	33°C		−12°C	
% of occurrence	3.35%	10.67%	3.43%	2.48%
% of change	+219%		−28%	
$\mu \pm 2\sigma$ criteria	33.8°C		−12.4°C	
% of occurrence	1.90%	4.32%	4.02%	2.96%
% of change	+127%		−26%	

period (2029-2064), a significant increase in the daily maximum temperature is expected in winter and in fall, while the daily maximum temperatures in spring and summer do not exhibit any significant change. On the other hand, variance in the future annual evolution of daily maximum temperature is expected to increase substantially throughout the year.

Figure 8 shows the future changes in the mean and variance for daily maximum, mean, and minimum temperatures in each season. As can be seen in the figure, seasonal average temperature is predicted to increase in summer, fall and winter,

and is expected to decrease in spring. The standard deviation of temperatures is predicted to rise in all seasons, which is already evident in Fig. 7. Spring is the only season to be predicted cooler. Future warming is highest in fall. While the temperature increase in summer is relatively insignificant, the increase in its standard deviation is remarkable; extreme hot events may occur more often in summer in future. While the standard deviation is expected to increase remarkably in summer, it is noted that the standard deviation of winter temperature is still greater than that of summer temperature. Springtime cooling is slightly weaker than shown in Fig. 8 when the 1961-2014 daily temperatures are used, but the difference is less than half a degree (figure not shown).

In Fig. 9, the histograms of maximum, average, and minimum daily temperature show similar trends as in Fig. 8. In spring, a small amount of cooling occurs in future, while warming occurs in other seasons. Note that the summer histogram becomes wider in both directions, while fall and winter histograms become shifted toward the warm side. This indicates that occurrence of extreme hot events will increase in future in summer, fall and winter, whereas extreme cold events will increase in summer but decrease in fall and winter.

The occurrence of extreme hot/cold events is portrayed in Table 2. Extreme events defined by both the KMA criteria and the 2σ (standard deviation) criteria are shown in Table 2; note that the KMA criteria and the standard-deviation criteria are slightly different in terms of the extreme values. In summer, extreme hot events tend to increase significantly in future,

Fig. 10. General Extreme Value (GEV) distribution and Generalized Pareto Distribution (GPD) of cold extremes (first and third columns) and warm extremes (second and fourth columns) during summer (6/1-8/31; first and second columns) and winter (12/1-2/28; third and fourth columns) based on the 100 synthetic datasets: observational period 1979-2014 (blue) and future period 2029-2064 (red). Warm and cold extreme are determined by the $\mu \pm 2\sigma$ values of the present data.

while extreme cold events tend to decrease slightly in winter. The occurrence of heat waves in summer tends to increase by ~220% according to the KMA criteria (maximum temperature over 33°C), and by ~130% according to the $\mu + 2\sigma$ criteria. In contrast, the occurrence of cold waves in winter tends to decrease by ~28% according to the KMA criteria (minimum temperature below –12°C) and by ~26% according to the $\mu - 2\sigma$ criteria. This is consistent with other results in this study.

The probability distribution of extreme values is shown in Fig. 10. Both the GEV distribution and the GPD are displayed in the figure. The probability density function of the GEV distribution is given by

$$f_{\text{GEV}}(x; \mu, \sigma, \xi) = \frac{1}{\sigma} t(x)^{-(1+\xi)} e^{-t(x)}, \tag{8}$$

where

$$t(x) = \begin{cases} \left(1 + \xi\left(\frac{x-\mu}{\sigma}\right)\right)^{-1/\xi} & \text{for } \xi \neq 0 \\ \exp\left(-\frac{x-\mu}{\sigma}\right), & \text{for } \xi = 0 \end{cases}, \tag{9}$$

and

$$\begin{cases} x > \mu - \sigma/\xi & \text{for } \xi > 0 \\ x < \mu - \sigma/\xi & \text{for } \xi < 0 \end{cases}. \tag{10}$$

Here, μ is the relocation parameter, $\sigma > 0$ is the scale parameter, and ξ is the shape parameter. The probability function of the GPD distribution is defined by
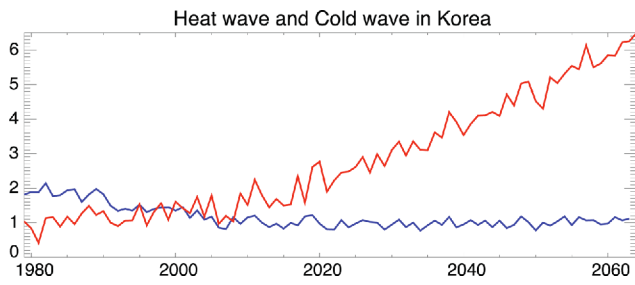
$$f_{\text{GPD}}(x; \xi, \mu, \sigma) = \frac{1}{\sigma}\left(1 + \frac{\xi(x-\mu)}{\sigma}\right)^{-\frac{1}{\xi}-1}, \tag{11}$$
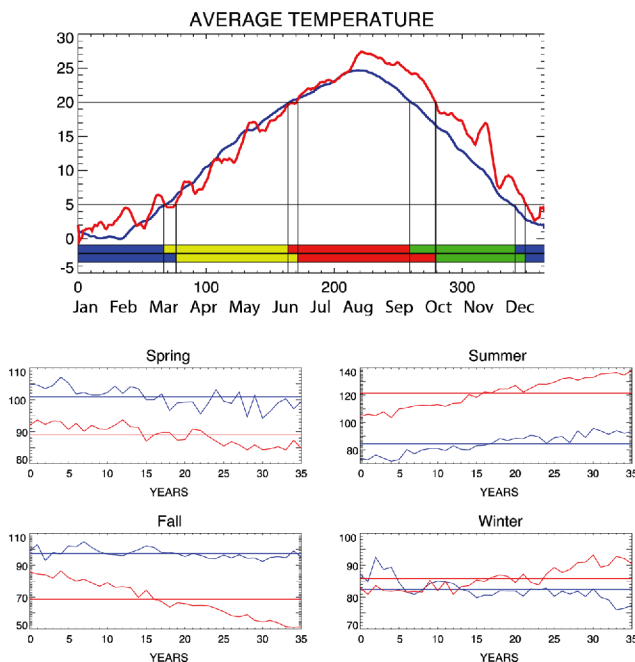
where

$$\begin{cases} x \geq \mu & \text{for } \xi \geq 0 \\ \mu \leq x \leq \mu - \sigma/\xi & \text{for } \xi < 0 \end{cases}. \tag{12}$$

Both the GEV and GPD distributions show similar distributions for the warm and cold extremes in summer and winter. For GPD distribution, extreme events are defined as the temperatures exceeding 2σ range ($\mu + 2\sigma$). For GEV distribution, block extrema (maximum and minimum temperatures

Fig. 11. Current and future trends of heat waves and cold waves in Korea. Days with daily maximum temperature exceeding 33°C for two or more consecutive days are defined as days of heat waves (red). Days with daily minimum temperatures below −12°C for two or more consecutive days or days with a temperature reduction of more than 10°C per day from a minimum temperature of 3°C or lower are defined as days of cold waves.

Fig. 12. (upper panel) The seasonal cycle of daily average temperatures. The color bars in the upper row depict the lengths of the seasons in 1979-2014, while those in the lower row describe the lengths of the seasons in 2029-2064. Each color represents the duration of a season: spring (yellow), summer (red), fall (green), and winter (blue). The seasonal cycles have been smoothed significantly in order to apply the KMA definitions of seasons. (lower panel) Plot of the length of each season during the observational period (1979-2014, blue) and the future period (2029-2064, red).

each year) are used. In order to facilitate a comparison, GEV distributions are plotted for values exceeding 2σ. As seen in the figure, both the warm and cold extremes will be more frequent in summer. In winter, warm extremes will be more frequent and anomalous, while occurrence of cold extremes, which stands for cold waves, will be similar to that in the present period.

Table 3. Mean and standard deviation of the length of each season derived form the 100 synthetic datasets. And start of each season also derived form 100 synthetic datasets. Seasonal criteria follow KMA criteria.

	Mean of Length (Days)	Standard Deviation	Start of Season (Date)
Spring (1979-2014)	100.02	3.52	3/26
Spring (2029-2064)	89.03	2.51	4/1
Summer (1979-2014)	84.37	3.85	7/3
Summer (2029-2064)	121.46	3.79	6/27
Fall (1979-2014)	97.40	3.88	9/27
Fall (2029-2064)	68.62	4.85	10/27
Winter (1979-2014)	82.40	3.48	1/4
Winter (2029-2064)	85.87	4.18	1/6

Figure 11 shows the predicted yearly occurrence of heat waves and cold waves in Korea; heat and cold waves are defined according to the KMA criteria. Heat waves will increase significantly in number in future, while cold waves will decrease slightly in number. Note that the changes in these two extreme events are not symmetric at all due to regional warming and seasonally distinct change in temperature variability. The rate of increase in heat waves is much greater than the rate of decrease in cold waves. The asymmetric trend is obvious, since the average temperature will be higher in future period due to global warming, and also the rate of increase in temperature variability (standard deviation) will be higher in summer.

Figure 12 and Table 3 show the future change in the onset date and length of each season. Season is defined according to the KMA classification, which is based on daily temperatures. According to the KMA classification, spring starts from the day when average temperature becomes higher than 5°C and afterward in the season. Summer starts from the day when average temperature becomes higher than 20°C and afterward in the season. Fall starts from the day when average temperature becomes lower than 20°C and afterward in the season. Winter starts from the day when average temperature becomes lower than 5°C and afterward in the season. The onset dates of the four seasons will be delayed by a few days according to the prediction datasets. Summer and winter, particularly summer, will be longer, while spring and fall, particularly fall, will become shorter.

4. Summary and Conclusions

Daily maximum, minimum, and average temperatures over the last 36 years (1979-2014) measured at the 60 KMA

stations in South Korea were analyzed via the CSEOF technique to construct synthetic datasets until 2064. The synthetic datasets were constructed by using the first 20 CSEOF modes, which explain more than 90 percent of the total variability. Synthetic PC time series were constructed from the autoregressive (AR) models fitted to the detrended PC time series and the linear trend in each PC time series. Then, daily temperatures for the future 50 years (2015-2064) have been studied using 100 synthetic datasets.

The accuracy of the synthetic datasets was validated against the original data in terms of the proximity of the underlying statistical properties. Both the mean and variance of the synthetic datasets were similar to those of the observational data. Also, the envelope of the 100 synthetic datasets in 1979-2014 showed a trend similar to that of the observational data.

In the future period (2029-2064), the first CSEOF mode (seasonal cycle) becomes weaker while the second CSEOF mode (warming) becomes stronger. According to the synthetic datasets, temperature is increased in summer, fall and winter while it is decreased slightly in spring. It seems that delay (Dwyer et al., 2012; Meehl et al., 2007) and weakening of the seasonal cycle (Serreze et al., 2009; Lynch et al., 2016) offers a plausible explanation for the springtime cooling in Korea; unfortunately, this cannot be confirmed based on a rather statistical approach in the present study.

On the other hand, standard deviation of daily temperatures increases in each season; the amount of increase in the standard deviation is greatest in summer, while the actual standard deviation of daily temperature remains to be greatest in winter both in the current and future periods. Histograms of daily temperatures are shifted toward the positive side in summer, fall, and winter; this indicates that warming will persist in future. In spring, however, histogram expands in both directions, suggesting that colder and warmer weathers will be more frequent in future.

From the 100 synthetic datasets, probability and frequency of extreme events are predicted using the generalized extreme value (GEV) distribution and the general Pareto distribution (GPD). The GEV and GPD methods yield similar results. The extreme value distribution as represented by GEV and GPD shows that extreme hot events (heat waves) will be more intense and more frequent, while extreme cold events (cold waves) will be slightly less intense and less frequent. The future trend of extreme events based on the KMA criteria for heat/cold waves shows that heat wave events will increase significantly in number, while cold wave events will decrease slightly. These two trends, heat waves and cold waves, are not symmetric at all due to the seasonally distinct change in the mean and variance of daily temperatures. The increase in the number of heat waves is larger than the number of reduction of cold waves.

The onset date and length of each season according to the KMA classification also change significantly in future. Summer and winter will become longer, while spring and fall will become shorter.

An important caveat in the present study is that (1) the linear trend in the PC time series will continue in future, and (2) the CSEOF loading vector will not change in any significant manner in future. It is impossible to ascertain that these two assumptions will be rigorously met in future. In fact, model predictions also suffer from unknown future forcing and/or uncertainty arising from unaffirmed model physics. Therefore, this study may be viewed as a simplistic prediction on future trend of daily temperature and its variability based on observational data, and serves as a benchmark solution for more complex numerical predictions.

Edited by: Kyong-Hwan Seo

References

Beniston, M., and Coauthors, 2007: Future extreme events in European climate: An exploration of regional climate model projections. *Climatic Change*, **81**, 71-95.

Bonsal, B. R., X. Zhang, L. A. Vincent, and W. D. Hogg, 2001: Characteristics of daily and extreme temperatures over Canada. *J. Climate,* **14**, 1959-1976.

Dwyer, J. G., M. Biasutti, and A. H. Sobel, 2012: Projected changes in the seasonal cycle of surface temperature. *J. Climate*, **25**, 6359-6374, doi:10.1175/JCLI-D-11-00741.1.

Easterling, D. R., J. L. Evans, P. Y. Groisman, T. R. Karl, K. E. Kunkel, and P. Ambenje, 2000: Observed variability and trends in extreme climate events: A brief review. *Bull. Amer. Meteor. Soc.*, **81**, 417-425.

Gilleland, E., and R. W. Katz, 2005: Extremes Toolkit (extRemes): Weather and climate applications of extreme value statistics. [Available online at http://www.isse.ucar.edu/extremevalues/evtk.html.]

Griffiths, G. M., and Coauthors, 2005: Change in mean temperature as a predictor of extreme temperature change in Asia - Pacific region. *Int. J. Climatol.*, **25**, 1301-1330, doi: 10.1002/joc.1194.

Houghton, J. T., Y. Ding, D. J. Griggs, M. Noguer, P. J. van der Linden, X. Dai, K. Maskell, and C. A. Johnson, 2001: *Climate Change 2001: The Scientific Basis.* Cambridge University Press, 944 pp.

Jung, H.-S., Y. G. Choi, J.-H. Oh, and G.-H. Lim, 2002: Recent trend in temperature and precipitation over South Korea. *Int. J. Climatol.,* **22**, 1327-1337, doi:10.1002/joc.797.

Katz, R. W., and B. G. Brown, 1992: Extreme events in a changing climate: Variability is more important than averages. *Climatic Change,* **21**, 289-302, doi:10.1007/BF00139728.

Kim, K.-Y., G. R. North, and J. Huang, 1996: EOFs of one-dimensional cyclostationary time series: Computations, examples and stochastic modeling. *J. Atmos. Sci.*, **53**, 1007-1017.

_____, and _____, 1997: EOFs of harmonizable cyclostationary processes. *J. Atmos. Sci.,* **54**, 2416-2427.

_____, and Q. Wu, 1999: A comparison study of EOF techniques: Analysis of nonstationary data with periodic statistics. *J. Climate*, **12**, 185-199.

_____, and J.-W. Roh, 2010: Physical mechanisms of the wintertime surface air temperature variability in South Korea and the near-7-Day oscillations. *J. Climate*, **23**, 2197-2212, doi:10.1175/2009JCLI3348.1.

_____, B. Hamlington, and H. Na, 2015: Theoretical foundation of

cyclostationary EOF analysis for geophysical and climatic variables: Concepts and examples. *Earth Sci. Rev.,* **150**, 201-218, doi:10.1016/j.earscirev.2015.06.003.

Kim, Y., K.-Y. Kim, and B.-M. Kim, 2013a: Physical mechanisms of European winter snow cover variability and its relationship to the NAO. *Climate Dyn.*, **40**, 1657-1669, doi:10.1007/s00382-012-1365-5.

_____, _____, and J.-G. Jhun, 2013b: Seasonal evolution mechanism of the East Asian winter monsoon and its interannual variability. *Climate Dyn.*, **41**, 1213-1228, doi:10.1007/s00382-012-1491-0.

_____, _____, and S. Park, 2014: Seasonal scale variability of the East Asian winter monsoon an the development of a two-dimensional monsoon index. *Climate Dyn.*, **42**, 2159-2172, doi:10.1007/s00382-013-1724-x.

Luterbacher, J., D. Dietrich, E. Xoplaki, M. Grosjean, and H. Wanner, 2004: Europian seasonal and annual temperature variability, trends and extreme since 1500. *Science,* **303**, 1499-1503, doi:10.1126/science.1093877.

Lynch, C., A. Seth, and J. Thibeault, 2016: Recent and projected annual cycles of temperature and precipitation in the Northeast United States from CMIP5. *J. Climate*, **29**, 347-365, doi:10.1175/JCLI-D-14-00781.1.

Mearns, L. O., R. W. Katz, and S. H. Schneider, 1984: Extreme high temperature events: changes in their probabilities with changes in mean temperature. *J. Climate Appl. Meteor.*, **23**, 1601-1613.

Meehl, G., C. Covey, T. Delworth, M. Latif, B. McAvaney, J. Mitchell, R. Stouffer, and K. Taylor, 2007: The WCRP CMIP3 multi-model dataset. *Bull. Amer. Meteor. Soc.,* **88**, 1383-1394.

Newton, H. J., 1988: *TIMESLAB: A Time Series Analysis Laboratory.* Brooks/Cole Pub Co, 625 pp.

Parkinson, C. L., 1994: Spatial patterns in the length of the sea ice season in the Southern Ocean, 1979-1986. *J. Geophys. Res.*, **99**, 16327-16339.

Robeson, S. M., 2002: Increasing growing-season length in Illinois during the 20th century. *Climatic Change,* **52**, 219-238.

Schär, C., P. L. Vidale, D. Lüthi, C. Frei, C. Häberli, M. A. Liniger, and C. Appenzeller, 2004: The role of increasing temperature variability in European summer heat waves. *Nature,* **427**, 332-336, doi:10.1038/nature02300.

Serreze, M. C., A. P. Barrett, J. C. Stroeve, D. N. Kindig, and M. M. Holland, 2009: The emergence of surface-based Arctic amplification. *The Cryosphere*, **3**, 11-19.

Walsh, J. E., A. S. Phillips, D. H. Portis, and W. L. Chapman, 2001: Extreme cold outbreaks in the United States and Europe, 1948-99. *J. Climate*, **14**, 2642-2658.